PNAS RESEARCH ARTICLE | APPLIED BIOLOGICAL SCIENCES

Decreasing the intrinsically disordered protein α-synuclein levels by targeting its structured mRNA with a ribonuclease-targeting chimera

Yuquan Tong[a,b,1], Peiyuan Zhang[a,1], Xueyi Yang[a,b], Xiaohui Liu[a], Jie Zhang[c,d], Magda Grudniewska[c,d], Ikrak Jung[c,d], Daniel Abegg[a], Jun Liu[c,d], Jessica L. Childs-Disney[a,b], Quentin M. R. Gibaut[a,b], Hafeez S. Haniff[a], Alexander Adibekian[a], M. Maral Mouradian[c,d], and Matthew D. Disney[a,b,2]

Edited by Marc I. Diamond, The University of Texas Southwestern Medical Center Medical School, Dallas, TX; received April 26, 2023; accepted November 21, 2023 by Editorial Board Member Lila M. Gierasch

α-Synuclein is an important drug target for the treatment of Parkinson's disease (PD), but it is an intrinsically disordered protein lacking typical small-molecule binding pockets. In contrast, the encoding *SNCA* mRNA has regions of ordered structure in its 5′ untranslated region (UTR). Here, we present an integrated approach to identify small molecules that bind this structured region and inhibit α-synuclein translation. A drug-like, RNA-focused compound collection was studied for binding to the 5′ UTR of *SNCA* mRNA, affording Synucleozid-2.0, a drug-like small molecule that decreases α-synuclein levels by inhibiting ribosomes from assembling onto *SNCA* mRNA. This RNA-binding small molecule was converted into a ribonuclease-targeting chimera (RiboTAC) to degrade cellular *SNCA* mRNA. RNA-seq and proteomics studies demonstrated that the RiboTAC (Syn-RiboTAC) selectively degraded *SNCA* mRNA to reduce its protein levels, affording a fivefold enhancement of cytoprotective effects as compared to Synucleozid-2.0. As observed in many diseases, transcriptome-wide changes in RNA expression are observed in PD. Syn-RiboTAC also rescued the expression of ~50% of genes that were abnormally expressed in dopaminergic neurons differentiated from PD patient–derived iPSCs. These studies demonstrate that the druggability of the proteome can be expanded greatly by targeting the encoding mRNAs with both small molecule binders and RiboTAC degraders.

RNA | parkinsonism | α-synuclein | Alzheimer's | targeted degradation

Genome-wide analyses suggest that only 15% of proteins are in druggable families (1, 2). A goal of chemical biology and medicinal chemistry, therefore, is to expand the druggable space by developing new approaches to target "undruggable" proteins that typically do not have architectures that are compatible with small-molecule binding. Current strategies to expand druggability include the use of proteolysis-targeting chimeras (ProTACs) to degrade protein targets (3–7) and covalent chemistry to define ligands that bind to shallow pockets, for example in mutant *KRAS* (8–11) and others (12, 13).

The protein α-synuclein is central to the pathogenesis of Parkinson's disease (PD) and other α-synucleinopathies, as it misfolds, oligomerizes, and forms fibrils (14). These fibrils propagate across neurons, aggregate in Lewy bodies and Lewy neurites, and are associated with neuronal degeneration (Fig. 1*A*) (15). A major factor that promotes α-synuclein fibrillization is its concentration, as individuals with multiplication of the *SNCA* gene locus develop dominantly inherited PD with a gene dosage effect (16). Thus, reducing the levels of α-synuclein protein is a potential disease-modifying strategy (17). However, as an intrinsically disordered protein (IDP) that lacks pockets that can typically be bound by small molecules, α-synuclein protein is considered undruggable (18, 19).

One promising strategy to expand protein druggability, particularly for disease-causing proteins that are overexpressed, is to target their coding mRNAs and inhibit translation (21, 22). Such an approach could be accomplished by defining structured regions in an mRNA as potential small-molecule binding pockets, followed by the identification of small molecules that bind these structures. Previously, we designed a small molecule named Synucleozid-1.0 (20) that selectively targets the iron-responsive element (IRE) in the 5′ untranslated region (5′ UTR) of *SNCA* mRNA (23), which encodes α-synuclein (Fig. 1*A*). The IRE is bound and stabilized by iron regulatory proteins (IRPs) at low iron concentrations, leading to repression of *SNCA* mRNA translation (24). At higher concentrations of iron, the IRPs are bound to iron rather than the *SNCA* IRE, increasing the accessibility of the mRNA to the translational machinery. The small molecule Synucleozid-1.0 stabilizes the *SNCA* IRE structure and is a functional surrogate for the cellularly expressed IRP that regulates the amount of *SNCA* mRNA loaded into polysomes. However, Synucleozid-1.0 did not have ideal physicochemical properties for CNS penetration (25).

Significance

Parkinson's disease can be caused by elevated levels of α-synuclein, an intrinsically disordered protein lacking typical small-molecule binding pockets. Here, we present an integrated approach to define drug-like chemical matter that targets its mRNA by simple binding and by targeted degradation to reduce α-synuclein protein levels in patient-derived neurons. Collectively, our work demonstrates that "undruggable" proteins can be targeted by binding to the encoding mRNA with small molecules. Further, we show that conversion of an RNA binder into a ribonuclease-targeting chimera can significantly enhance its potency while retaining selectivity on the transcriptome and proteome. Broadly, this platform can be used to expand the druggability of many challenging disease targets.

Author contributions: J.L.C.-D. and M.D.D. designed research; Y.T., P.Z., X.Y., X.L., J.Z., M.G., I.J., D.A., J.L., Q.M.R.G., and H.S.H. performed research; Y.T., P.Z., X.Y., X.L., D.A., and A.A. analyzed data; and Y.T., P.Z., J.L.C.-D., M.M.M, and M.D.D. wrote the paper.

Competing interest statement: M.D.D. is a founder of Expansion Therapeutics. M.M.M. is a founder of MentiNova.

This article is a PNAS Direct Submission. M.I.D. is a guest editor invited by the Editorial Board.

[1]Y.T. and P.Z. contributed equally to this work.

[2]To whom correspondence may be addressed. Email: mdisney@ufl.edu.

This article contains supporting information online at https://www.pnas.org/lookup/suppl/doi:10.1073/pnas.2306682120/-/DCSupplemental.

Published January 5, 2024.

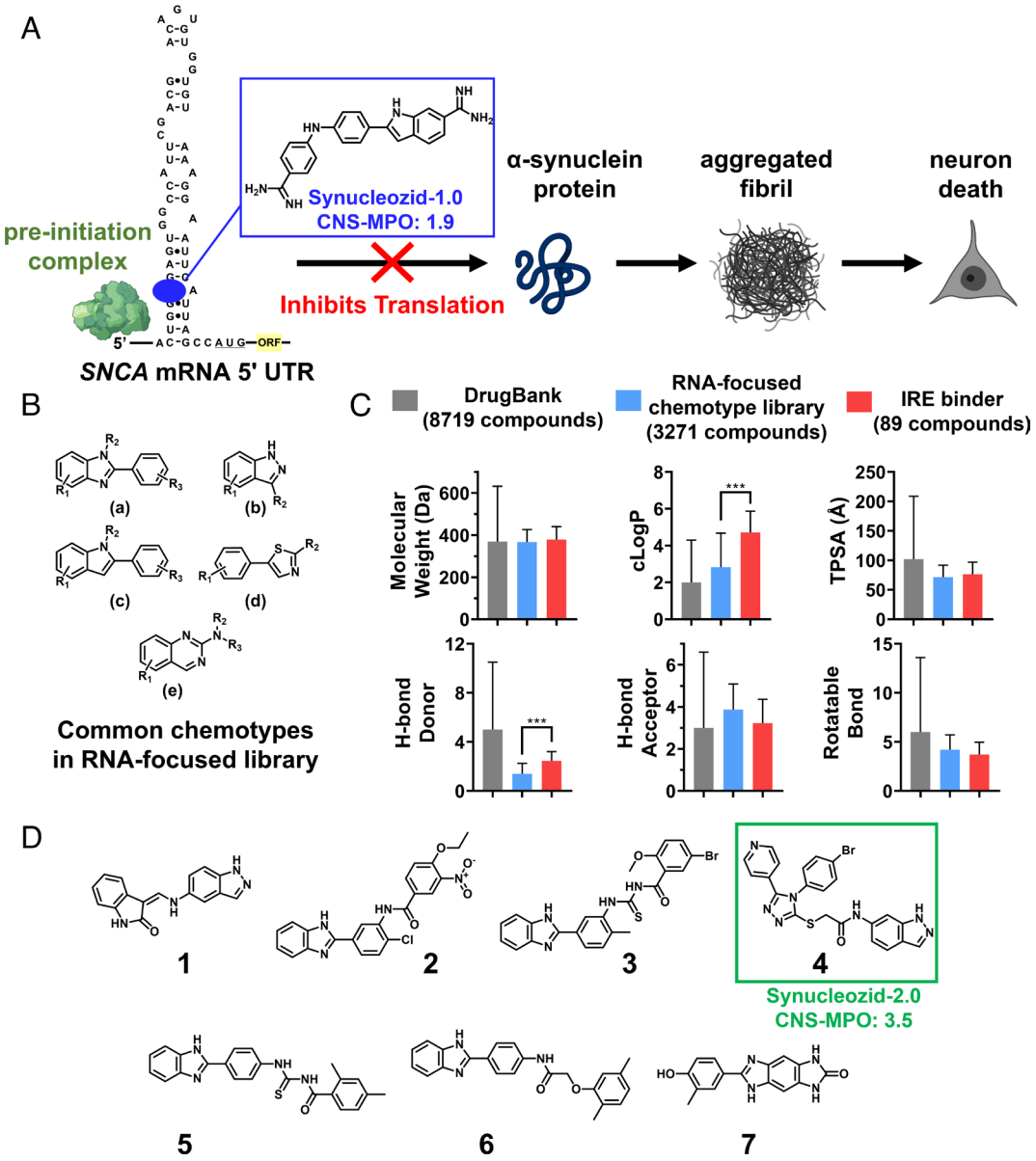

Fig. 1. Schematic depiction of α-synuclein-mediated disease pathway shows small molecules targeting the *SNCA* IRE can inhibit α-synuclein translation. (*A*) α-synuclein can misfold and form fibrils that propagate across neurons in the brain, accumulate in Lewy bodies, and lead to neuronal death. The IRE harbored in the 5′ UTR of *SNCA* mRNA regulates α-synuclein translation. Synucleozid-1.0 is a small molecule that we previously identified to bind the *SNCA* IRE A bulge and inhibit α-synuclein translation (20). (*B*) RNA-focused chemotype library containing (*a*) 2-phenyl-1,3-benzimidazoles, (*b*) 1,2-benzimidazoles, (*c*) 2-phenyl indoles, (*d*) 4-phenyl thiazoles, and (*e*) 2-amino quinazolines screened for binding to the *SNCA* IRE. (*C*) Comparison of the physiochemical properties of 8,719 cataloged drugs in DrugBank, 3,271 compounds in the RNA-focused library, and 89 hit compounds from the RNA-focused library that bind the *SNCA* IRE. (*D*) Chemical structures of seven small molecules that down-regulate α-synuclein levels in SH-SY5Y cells identified by Western blotting out of the 89 hit compounds. ***$P < 0.001$, as determined by two-tailed Student *t* test. Error bars indicate SD.

In the current study, we lay a foundation to discover small molecules that target RNA by using several synergistic approaches to define novel chemical matter with favorable drug-like physicochemical properties, as applied to *SNCA* mRNA (*SI Appendix*, Fig. S1*A*). First, we designed and delivered RNA-focused small molecules by informatic analysis of all known small-molecule-RNA fold interactions housed in our lead identification software, Inforna (26). These small molecules were screened for binding to the *SNCA* IRE using a microarray approach in which the small molecules are noncovalently absorbed onto the surface. Dubbed AbsorbArray, this method allowed for the facile screening of compounds for binding to the *SNCA* IRE, defining drug-like and selective lead small molecule binders (27). Biological investigations demonstrated direct RNA target engagement and defined the small molecule's binding site. These synergistic methods defined the druggable pockets within the *SNCA* 5′ UTR and delivered a unique bioactive compound, dubbed Synucleozid-2.0, with improved potency, selectivity, and drug-like physicochemical properties compared to Synucleozid-1.0 (25). We have also mechanistically defined the small molecule's mode of action where it inhibits the assembly of actively translating ribosomes onto the *SNCA* mRNA.

To further enhance the potency, we converted Synucleozid-2.0 into an RNA degrader by tethering it with a ribonuclease-recruiting module, affording a ribonuclease-targeting chimera (RiboTAC). Named Syn-RiboTAC, the degrader molecule's cytoprotective effect was fivefold greater than Synucleozid-2.0. Transcriptome- and proteome-wide studies confirmed that both compounds selectively target *SNCA* mRNA in cells and reduce α-synuclein expression levels in PD patient–derived dopaminergic neurons differentiated from induced pluripotent stem cells (iPSCs).

Results and Discussion

RNA-Focused Small Molecules Bind to the *SNCA* IRE. Previously, we constructed an RNA-focused, drug-like small molecule library (28) by analyzing the physicochemical properties of all known RNA-binding small molecules (26). The 1.3 million compounds in the Chembridge Core and Express Libraries were mined for diverse small molecules with similar properties, affording a collection of 3,271 drug-like small molecules biased for binding RNA. Common chemotypes in the library include 2-phenyl-1,3-benzimidazoles, 1,2-benzimidazoles, 2-phenyl indoles, 4-phenyl thiazoles, and 2-amino quinazolines (Fig. 1*B*). Comparison of the properties of RNA-focused library to the properties of known drugs shows that overall they are similar with modest differences in hydrophobic surface area and the number of hydrogen bond donors (Fig. 1*C*).

The RNA-focused library was evaluated for binding to the *SNCA* IRE target by using small molecule microarrays, particularly AbsorbArray where compounds are absorbed onto an agarose-coated microarray (27). AbsorbArray expedites the construction and screening of arrays as it does not require installation of an orthogonal reactive handle for immobilization, which can obscure binding if the modification removes key interactions with the RNA target. The array surface was incubated with ^{32}P-labeled IRE RNA in the presence of excess unlabeled tRNA (competitor), affording 89 hit compounds (2.7% hit rate) that selectively bound the *SNCA* IRE (*SI Appendix*, Fig. S1*B*).

The structures of the compounds were analyzed informatically to define chemotypes that confer binding to the *SNCA* IRE. The enrichment of a particular scaffold in the binders as compared to the entire RNA-focused library and the statistical significance of that enrichment were calculated. This analysis defined eight different substructures that are biased for binding the *SNCA* IRE. The most statistically significant classes ($P < 0.01$) included benzimidazole, benzamidine, and imidazole-containing substructures (class 1 and class 2; *SI Appendix*, Fig. S1*B*). Not surprisingly, many of these scaffolds have previously been shown to interact with RNA (29–32). Other physicochemical properties that were enriched in the *SNCA* IRE binders relative to the starting RNA-focused library include a modestly increased cLogP and an increased number of hydrogen bond donors (Fig. 1*C*).

Compounds That Bind the *SNCA* IRE Inhibit Its Translation. It is difficult to design or discover bioactive ligands that bind RNA and affect target-mediated processes; an even greater challenge is to define the mechanistic underpinnings of such compounds. Therefore, we conducted a screening cascade on candidate compounds that bind the *SNCA IRE* to identify those that are bioactive and to provide experimental support for their mode of action (*SI Appendix*, Fig. S1*A*).

The 89 small molecules (2 μM) that bind the *SNCA* IRE were evaluated for inhibiting α-synuclein translation in SH-SY5Y cells, a human dopaminergic neuroblastoma cell line commonly used to study the expression of α-synuclein, by Western blotting (*SI Appendix*, Fig. S2) (33). Seven decreased the levels of α-synuclein, by more than 40%, and all compounds were well tolerated by the cells (Fig. 1*D* and *SI Appendix*, Fig. S3 *A*–*C*).

Reduction of α-synuclein protein levels can be due to several factors and can be independent of binding to the *SNCA* IRE. To gain insight into whether compound activity is due to selective recognition of the IRE, we used a luciferase reporter with or without *SNCA* 5′ UTR that harbors the IRE. Four compounds, **2**, **4**, **6**, and **7**, selectively inhibited translation of luciferase when fused to the *SNCA* 5′ UTR; that is, they had no effect on translation of luciferase lacking the IRE (Fig. 2*A* and *SI Appendix*, Fig. S3 *D* and *E*). The next step in the screening cascade was to assess the effect of these small molecules on endogenous *SNCA* mRNA levels in SH-SY5Y cells by using qRT-PCR. Compounds **2**, **4**, and **7** had no effect on *SNCA* mRNA levels and thus were carried forward; **6**, which reduced the mRNA levels, was removed from further consideration (Fig. 2*B* and *SI Appendix*, Fig. S3*F*). An inhibitory effect on *SNCA* translation can also occur if a small molecule increases IRP levels, as IRPs are negative regulators of *SNCA* translation (34). Compounds **4** and **7** had no effect on IRP-1 or IRP-2 levels. Compound **2**, on the other hand, increased IRP-1 levels (but not IRP-2) and was therefore excluded from further study (*SI Appendix*, Fig. S3*G*).

Compounds That Inhibit *SNCA* Translation Protect against Cell Death Induced by α-Synuclein Preformed Fibrils. Preformed fibrils (PFFs) of α-synuclein prepared from recombinant human α-synuclein monomeric protein (35) seed aggregation and fibrillization of soluble endogenous α-synuclein when added to cells, triggering cellular damage and toxicity, which can be measured by lactate dehydrogenase (LDH) release (35). Small molecules **4** and **7** conferred cytoprotection from cytotoxicity upon PFF challenge, with **4** being more effective and providing protection at a dose as low as 2 μM (Fig. 2*C* and *SI Appendix*, Fig. S4*A*). Importantly, no toxicity was observed upon **4**-treatment in SH-SY5Y cells, as determined by LDH cytotoxicity assay (*SI Appendix*, Fig. S4*B*). As **4** (heretofore referred to as Synucleozid-2.0) was superior to **7**, we further characterized its activity and mechanism by which it inhibits translation. Note: Synucleozid-2.0 is a unique scaffold, a substituted indazole, different from Synucleozid-1.0, a di-guanidinylated substituted indole (Fig. 1 *A* and *D*).

Synucleozid-2.0 Specifically Inhibits *SNCA* IRE-Driven Translation in Cells. In SH-SY5Y cells, Synucleozid-2.0 dose-dependently inhibited *SNCA* translation with an IC_{50} of ~2 μM, as determined by Western blotting (Fig. 2*D* and *E*). To assess its specificity for the *SNCA* IRE vs. IRE-driven translation of other mRNAs, we studied its effect on ferritin and APP, both of which have an IRE in their 5′ UTR (24, 36), and TfR, which has an IRE in its 3′ UTR (Fig. 2 *D* and *E*) (37). Notably, these IREs have no structural overlap with the *SNCA* IRE (*SI Appendix*, Fig. S5), and Synucleozid-2.0 had no effect on their protein levels. Interestingly, Synucleozid-1.0, while potently decreasing α-synuclein levels, also had a modest effect on ferritin (20).

Synucleozid-2.0 Selectively Binds and Stabilizes the *SNCA* IRE In Vitro. We measured the binding affinity and selectivity of Synucleozid-2.0 using a previously described model of the IRE in which the A bulge was replaced with the fluorescent adenine mimic 2-aminopurine (2-AP) (20). The emission of 2-AP is dependent upon its microenvironment (38); thus, ligand binding can alter how 2-AP is stacked in a helix and change its fluorescence intensity (39, 40). This simple modification allows detection of small-molecule binding to the A bulge of the IRE. Indeed, Synucleozid-2.0 decreased 2-AP emission of the labeled IRE with an EC_{50} of 2.9 ± 0.4 μM (*SI Appendix*, Fig. S6*A*). Competitive binding assays were also completed with unlabeled wild-type (WT) *SNCA* IRE. Recovery of 2-AP emission was observed as a function of unlabeled WT IRE concentration, affording a competitive K_d of 1.8 ± 0.3 μM (*SI Appendix*, Fig. S6*B*). Thus, both 2-AP-labeled and WT IRE bind to Synucleozid-2.0 with similar affinities.

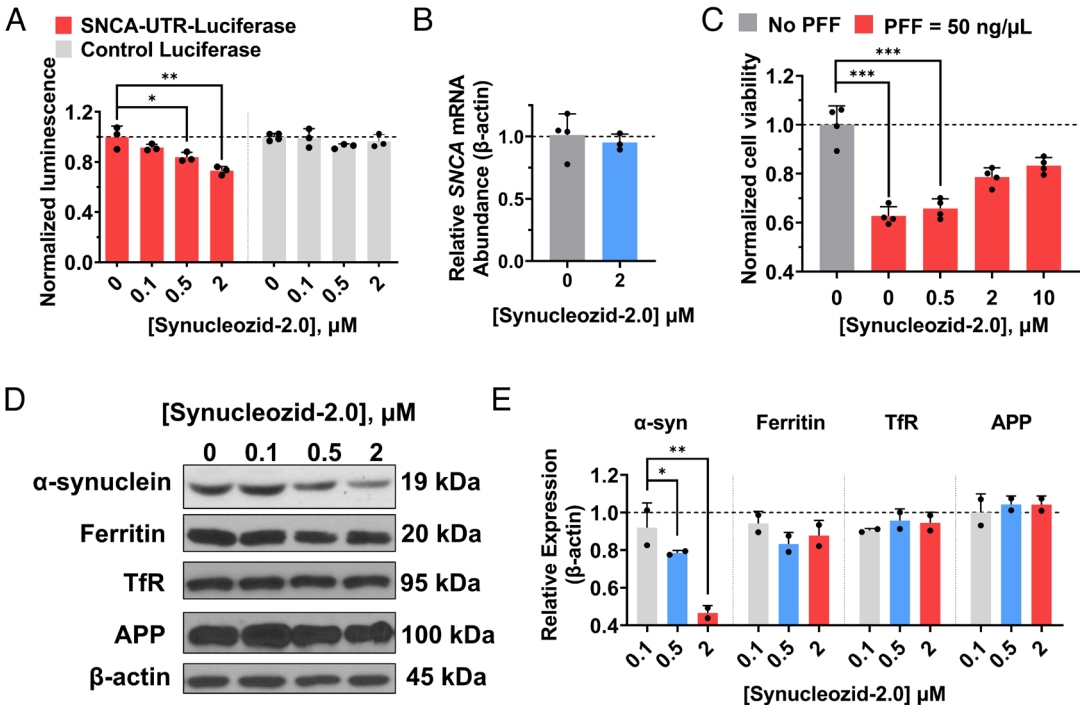

Fig. 2. Synucleozid-2.0 inhibits translation of *SNCA* mRNA and is cytoprotective in cells by selectively binding to the *SNCA* IRE region. (*A*) Effect of Synucleozid-2.0 (48 h) on translation of a luciferase reporter gene in HeLa cells with or without the *SNCA* 5′ UTR that harbors the IRE (n = 3 biological replicates for all conditions except vehicle-treated Control Luciferase reporter where n = 4). (*B*) Effect of Synucleozid-2.0 (48 h) on *SNCA* mRNA levels in native SH-SY5Y cells (n = 4 biological replicates for vehicle (0 μM) and n = 3 for Synucleozid-2.0 (2 μM)). (*C*) Cytoprotective effect after 48 h of Synucleozid-2.0 treatment of SH-SY5Y cells against 50 ng/μL human preformed fibrils (PFFs), a model of α-synuclein toxicity, measured by LDH assay (n = 4 biological replicates). PFFs act as seeds and recruit endogenous α-synuclein to aggregate. (*D*) Representative Western blot analysis for α-synuclein and other proteins that have IREs in the UTRs of their respective encoding mRNAs, including ferritin, TfR, and APP after treatment with Synucleozid-2.0 for 48 h. (*E*) Quantification of Western blot data, including those shown in D (n = 2 biological replicates). **P* < 0.05; ***P* < 0.01; ****P* < 0.001, as determined by two-tailed Student *t* test. Error bars indicate SD.

To study selectivity, we completed additional competition binding experiments with a series of 12 unlabeled RNAs into which mutations were introduced into the IRE. Each of RNA-1 to RNA-5 replaces one noncanonically paired region with base pairs (*SI Appendix*, Fig. S6*B*). Only RNA-1, in which the A bulge was mutated to an AU pair, reduced Synucleozid-2.0 binding, by 12-fold, while binding was unchanged in the presence of the other competitor RNAs. Thus, Synucleozid-2.0 has one binding site, the A bulge. Further, Synucleozid-2.0 did not bind fully base-paired RNA-6, with no significant recovery of 2-AP emission at 100 μM.

The selectivity of Synucleozid-2.0 for binding to the *SNCA* IRE A bulge was next assessed by introducing a point mutation to afford a G or U bulge (*SI Appendix*, Fig. S6*B*). The A bulge was not replaced with C as a significant structural rearrangement was predicted to occur. We also studied RNAs in which the A bulge's closing base pairs were altered. These mutated RNAs are designated as RNA-7 to RNA-12. Mutation of the A bulge to U or G (RNA-7 and RNA-8) reduced affinity of Synucleozid-2.0 by >10-fold. Interestingly, these bulges can be found in the ferritin, APP, and TfR IRE, and the lack of binding affinity is consistent with the inability of Synucleozid-2.0 to inhibit their translation (Fig. 2*D* and *E*). Mutating the closing base pairs to GC and AU (RNA-9 to RNA-12) reduced the small molecule's affinity by >12-fold (*SI Appendix*, Fig. S6*B*). Collectively, these experiments show that Synucleozid-2.0 recognizes the A bulge and its closing base pairs in *SNCA* IRE to confer selective binding by forming contacts with the three-dimensional structure within the RNA.

Synucleozid-2.0 Binds a Unique, Functional Site in the *SNCA* IRE. To verify these data, both in vitro and in cells, we employed antisense oligonucleotide ligand binding site mapping (ASO-Bind-Map), which provides a streamlined approach to define small-molecule-RNA binding sites (20). The ASO-Bind-Map approach was developed to provide a simple means to study small molecule binding and molecular recognition of RNA targets, including the specific binding site, without modification of the small molecule (20).

ASO-Bind-Map detects ligand binding sites by impeding the ability of oligonucleotides to hybridize to sites where the small molecule is bound, inspired by studies that used RNase H to investigate RNA folding (41). That is, small molecule binding thermodynamically stabilizes the RNA target at the binding site, inhibiting oligonucleotide hybridization (20). In contrast, oligonucleotides that hybridize outside of the small-molecule binding site are not affected and induce RNase H cleavage of the transcript. Thus, ASO-Bind-Map identifies the binding sites for small molecules to RNA in vitro and in cells. Knowledge of binding sites can help establish a mode of action and validate the target.

Detection of small-molecule binding sites by using ASO-Bind-Map can be completed in several formats. In vitro, a simple fluorescence resonance energy transfer (FRET) assay can be employed, particularly for RNA targets that fold into hairpin structures. The RNA is fluorescently labeled with FRET pairs on the 5′ and 3′ ends, generating a FRET signal when folded, i.e., a molecular beacon (*SI Appendix*, Fig. S7). Binding of an oligonucleotide to an RNA target disrupts the structure and causes a loss in FRET. The loss in FRET signal can be amplified when RNase H is added to the reaction as it cleaves the RNA strand in an RNA-DNA hybrid to cause irreversible disruption of structure upon cleavage. Small molecules that bind the same site as the oligonucleotide would prevent or reduce loss of the FRET signal.

In cells, inhibition of oligonucleotide binding due to small molecule stabilization of the target RNA is assessed by using qRT-PCR. Oligonucleotides (DNA or DNA gapmers) recruit endogenous cellular RNase H to cleave the RNA strand in an RNA–DNA hybrid

and deplete the target RNA (Fig. 3*A*). If the binding site of an oligonucleotide and that of a small molecule overlap, the target RNA is not cleaved or cleaved to a lesser extent, and its levels are restored. If these binding sites do not overlap, there is similar cleavage of the RNA target in the presence and absence of the small molecule.

Six tiling ASOs that bind throughout the *SNCA* IRE hairpin (*SI Appendix*, Table S1) were designed to define the binding site of Synucleozid-2.0. We first validated that each oligonucleotide induced RNase H cleavage in vitro using the FRET RNA sensor (*SI Appendix*, Fig. S8*A*). Synucleozid-2.0 inhibited RNase H cleavage triggered by ASO-1 and ASO-6, which overlap with the A bulge. (As an aside, 7 inhibited cleavage triggered by ASO-3, ASO-4, and ASO-5, indicating that this small molecule binds to the AGU hairpin loop and the adjacent GG bulge. These experiments defined two druggable pockets in the *SNCA* IRE mRNA that inhibit translation). Interestingly, Synucleozid-2.0 and Synucleozid-1.0 have the same binding site (20). To further support the notion that Synucleozid-2.0 binds and stabilizes the *SNCA* IRE as indicated by ASO-Bind-Map studies, thermal melting experiments were performed on WT *SNCA* IRE (RNA-0) and RNA-1 (in which the A bulge is mutated to an AU pair) in the presence or absence of Synucleozid-2.0. The compound stabilized the WT IRE, decreasing its ΔG°_{37} from −2.85 to −3.19 kcal/mol and increasing its T_m by 4 °C from 51.1 to 55.1 °C (*SI Appendix*, Fig. S8*B*).

We next investigated Synucleozid-2.0 binding site in cells using gapmer ASOs (2′-O-methoxyethyl [MOE] phosphorothioates) that are metabolically stable and overlap with the Synucleozid-2.0 binding site as determined from in vitro studies. A control gapmer of ASO-5 (Gapmer-5), which does not overlap with the Synucleozid-2.0 binding site, and a scrambled gapmer, which is not complementary to the *SNCA* mRNA, were also used in these cellular experiments (Fig. 3 *A* and *B* and *SI Appendix*, Table S1) (20). The three gapmers

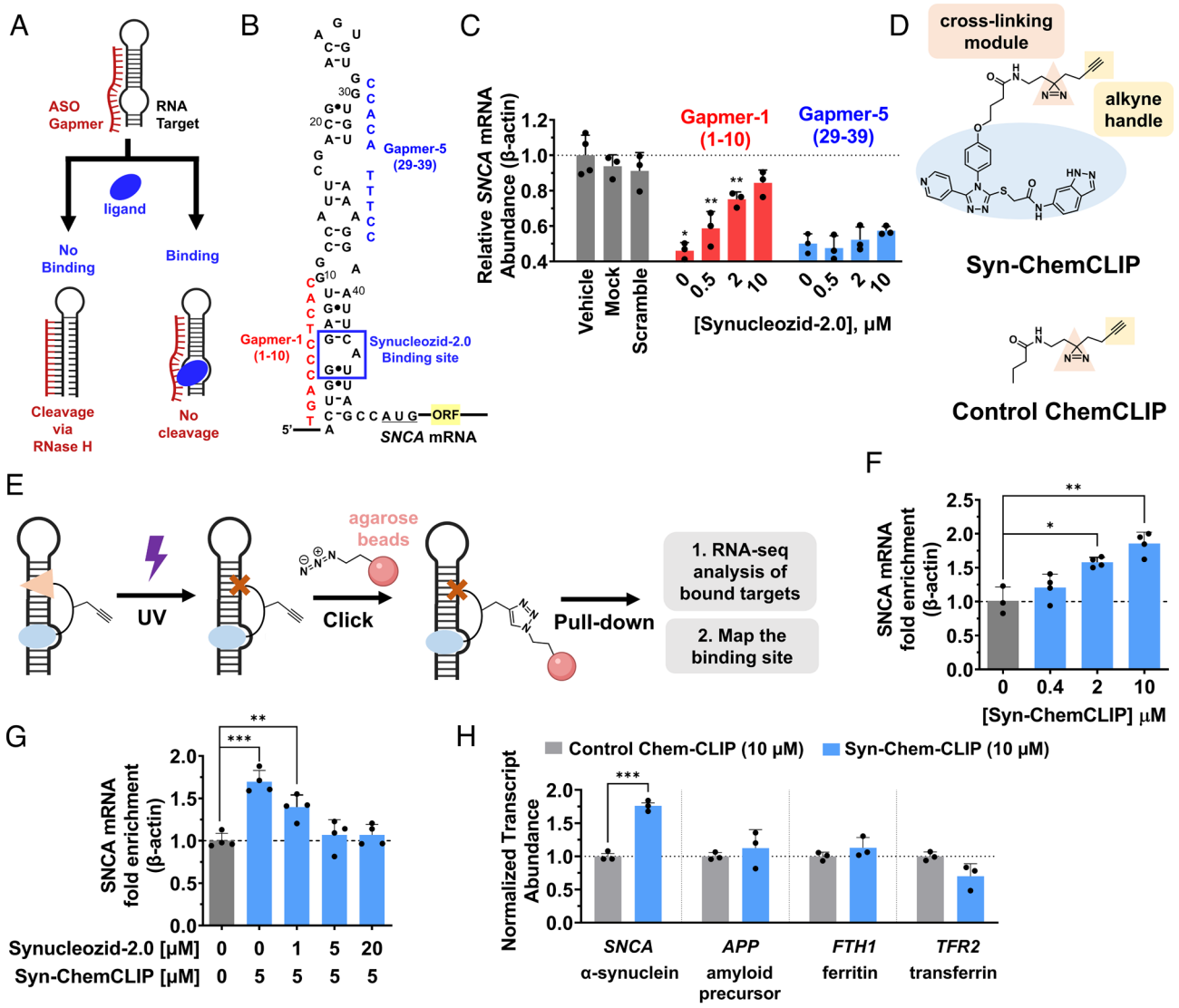

Fig. 3. Target validation and mapping of Synucleozid-2.0 for the *SNCA* IRE by Chem-CLIP. (*A*) Schematic depiction of cellular ASO-Bind-Map studies. (*B*) Gapmer sequences used in this study for the cellular ASO-Bind-Map. (*C*) Levels of *SNCA* mRNA in cells transfected with two designed Gapmers, in the presence or absence of Synucleozid-2.0 (48 h treatment; n = 3 biological replicates except for vehicle-treated samples where n = 4). Synucleozid-2.0 protects *SNCA* mRNA from RNase-mediated degradation by Gapmer-1, defining Synucleozid-2.0 binding site. No protection is observed by Gapmer-5, which hybridizes to a distal site. (*D*) Structure of the probe Syn-ChemCLIP (Chemical Cross-Linking and Isolation by Pull-down) for target validation and binding site mapping. (*E*) Schematic depiction of the Chem-CLIP workflow. (*F*) Syn-ChemCLIP dose-dependently enriched *SNCA* mRNA by cross-linking and pull-down in SH-SY5Y cells after a 16 h treatment period (n = 4 biological replicates except for vehicle-treated samples (0 μM) where n = 3). (*G*) Competitive Chem-CLIP (C-Chem-CLIP) showed that co-treatment of Synucleozid-2.0 dose-dependently ablated the enrichment of *SNCA* mRNA by Syn-ChemCLIP in SH-SY5Y cells (16 h treatment; n = 4 biological replicates). (*H*) Syn-ChemCLIP does not enrich other mRNA containing IRE regions, as determined by RNA-seq (16 h treatment; n = 3 biological replicates). **P* < 0.05; ***P* < 0.01, ****P* < 0.001, as determined by two-tailed Student *t* test. Error bars indicate SD.

were transfected into SH-SY5Y cells. As expected, Gapmer-1 and Gapmer-5, but not the scrambled control gapmer, cleaved the *SNCA* mRNA (Fig. 3*C*). Addition of increasing concentrations of Synucleozid-2.0 afforded dose-dependent inhibition of *SNCA* mRNA cleavage by Gapmer-1 but not Gapmer-5 or the scrambled control. Thus, ASO-Bind-Map studies showed direct target engagement in cells and that the site around the A bulge is bound, further supporting that Synucleozid-2.0 binds to the A bulge region of the *SNCA* IRE.

Cellular target engagement was further explored using an orthogonal target validation assay named Chemical Cross-Linking and Isolation by Pull-down (Chem-CLIP) (30). The probe used for these studies, Syn-ChemCLIP, was synthesized by tethering Synucleozid-2.0 with a photoactivatable diazirine group and an alkyne handle (Fig. 3*D*). Upon irradiation with UV light, the diazirine module reacts with its proximal targets to form covalent bonds, and the alkyne group enables click chemistry to beads for pull-down of the targets (Fig. 3*E*). Target enrichment is quantified by qRT-PCR. Indeed, dose-dependent enrichment of the *SNCA* mRNA was observed upon treatment of SH-SY5Y cells with Syn-ChemCLIP, with a 50% increase at 2 μM and a twofold increase with 10 μM, supporting direct target engagement (Fig. 3*F*). To confirm that Syn-ChemCLIP occupies the same binding site as its parent compound Synucleozid-2.0, competitive Chem-CLIP (C-Chem-CLIP) was performed. SH-SY5Y cells were co-treated with varying concentrations of Synucleozid-2.0 and a constant concentration of Syn-ChemCLIP (5 μM). As expected, increasing concentrations of Synucleozid-2.0 ablated enrichment by Syn-ChemCLIP, suggesting that both compounds compete for the same binding site within the *SNCA* mRNA (Fig. 3*G*). Notably, APP, TfR, and ferritin mRNAs were not enriched by Syn-ChemCLIP, as they do not share structural similarity with the *SNCA* IRE nor did Synucleozid-2.0 inhibit their translation (Figs. 2*E* and 3*H*).

We also used Syn-ChemCLIP to map the Synucleozid-2.0 binding site within the *SNCA* IRE in vitro. Cross-linking of the probe to the IRE impedes reverse transcription, and the exact location of the cross-link can be mapped by sequencing the truncated cDNA product (42). Consistent with results from ASO-Bind-Map studies, the cross-linking site of Syn-ChemCLIP was mapped to a guanosine residue that forms the G-U closing base pair of the targeted A bulge (*SI Appendix*, Fig. S8*C*). Collectively, both ASO-Bind-Map and Chem-CLIP validated direct target engagement of Synucleozid-2.0 in vitro and in cells, mapping its binding site to the A bulge in *SNCA* IRE.

Synucleozid-2.0 Acts by Inhibiting Assembly of Ribosomes onto *SNCA* mRNA. We explored several hypotheses related to Synucleozid-2.0's mode of action for inhibiting *SNCA* translation. First, we investigated whether Synucleozid-2.0 affects the molecular recognition of the *SNCA* IRE by IRP-1 and IRP-2 using an RNA immunoprecipitation (RIP) assay (*SI Appendix*, Fig. S9*A*). The amount of *SNCA* mRNA immunoprecipitated by IRP-1 or IRP-2 did not change upon treatment with Synucleozid-2.0 (*SI Appendix*, Fig. S9*B*), indicating that Synucleozid-2.0 did not interfere with the interactions between the IRPs and *SNCA* mRNA. The interaction between IRP-1 and *SNCA* IRE was, however, affected by iron concentration. Treatment of SH-SY5Y cells with iron (II) decreased the amount of *SNCA* mRNA pulled down in RIP fractions (*SI Appendix*, Fig. S9*B*), as expected since iron binds to IRP-1 and inhibits its interaction with the IRE. Conversely, treatment with the iron chelator deferoxamine (DFOA) (43) increased the amount of *SNCA* mRNA pulled down (*SI Appendix*, Fig. S9*B*). As IRP-2 expression is dependent on iron concentration (44), an ASO complementary to the IRP-2 binding site in the IRE was used as positive control and reduced the amount of *SNCA* mRNA in the pulled-down fractions (*SI Appendix*, Fig. S9*B*). These findings suggested that Synucleozid-2.0's mode of action is not blocking the association of *SNCA* mRNA with IRPs, in agreement with in vitro displacement assays (*SI Appendix*, Fig. S9 *C* and *D*).

Previous studies showed that Synucleozid-1.0, which shares its binding site with Synucleozid-2.0, affects ribosome assembly onto *SNCA* mRNA. We therefore investigated whether Synucleozid-2.0 operates by the same mode of action by using polysome profiling (*SI Appendix*, Fig. S10*A*) (20, 45). In polysome profiling, mRNAs are fractionated by how many ribosomes they are associated with using a sucrose gradient. An mRNA that is less translated is expected to have fewer ribosomes loaded onto it. Treatment of SH-SY5Y cells with Synucleozid-2.0 significantly shifted the distribution of *SNCA* mRNA associated with polysomes (fractions 8 to 14) to incomplete ribosomes (association with 40S or 60S subunits; fractions 1 to 5), with no significant change in the amount associated with single ribosomes (80S; fractions 5 to 7) (*SI Appendix*, Fig. S10 *B* and *C*). The significant increase of the fraction of *SNCA* mRNA complexed with incomplete ribosomes suggested that Synucleozid-2.0 inhibits translation during formation of the preinitiation complex (40S subunit and initiation factors) that scans from 5′ cap to the AUG start codon but not the elongation stage when single 80S ribosomes scan through the open reading frame (ORF; *SI Appendix*, Fig. S10*A*) (46).

Collectively, these experiments indicate that the translational inhibition of *SNCA* mRNA by Synucleozid-2.0 can be traced to stabilizing the IRE in the *SNCA* 5′ UTR, preventing its unfolding, and inhibiting ribosomal loading. This mechanism is akin to that observed for Synucleozid-1.0, which might be expected since both compounds bind the same structure within the *SNCA* IRE.

Bioactive Ligands Targeting *SNCA* IRE Have Drug-Like Physicochemical Properties. To assess the physicochemical properties of small molecules targeting *SNCA* mRNA in cells, we calculated Central Nervous System Multiple Parameter Optimization (CNS-MPO) scores, which predict blood–brain barrier (BBB) penetrance, a key pharmacological profile for the treatment of PD (47). The CNS-MPO score takes into account: i) lipophilicity (cLogP); ii) calculated distribution coefficient at pH 7.4 (cLogD); iii) molecular weight (MW); iv) topological polar surface area (TPSA); v) the number of hydrogen-bond donors (HBDs); and vi) the most basic center (pK_a) (47). Each parameter is equally weighted on a scale of 0 to 1 (based on comparison to known CNS-penetrant drugs) and summed. A score >4 indicates the small molecule is likely BBB penetrant. Synucleozid-1.0 has a CNS-MPO of 1.9 while Synucleozid-2.0 has a CNS-MPO of 3.5. Thus, the compound's drug-likeness has been improved substantially without sacrificing biological activity, selectivity, or compromising mode of action.

Converting Synucleozid-2.0 into a Ribonuclease-Targeting Chimera Enhances Its Cytoprotective Activity. One approach to enhance the potency of RNA binders is to tether them to a ribonuclease-recruiting small molecule, affording a ribonuclease-targeting chimera (RiboTAC) (48). The RNA-binding module drives the interaction with the *SNCA* IRE, while the ribonuclease-recruiting small-molecule module activates RNase L in proximity of the target RNA to induce its cleavage. Previous studies have shown that RiboTACs degrade the target substoichiometrically and are more selective (48, 49) than the RNA-binding small molecule from which they are derived. The observed enhancement in selectivity is a composite of the specificity of the RNA-binding

module, the substrate specificity of RNase L, and the juxtaposition of the binding site of the RNA-binding module to a site sensitive to RNase L cleavage (49).

Therefore, Synucleozid-2.0 was converted into Syn-RiboTAC by conjugation to a heterocyclic small molecule that recruits and activates RNase L (Fig. 4*A*). A control compound, Syn-CTRL (Fig. 4*A*), was also synthesized in which the RNase L-recruiting module was replaced with a regioisomer that is ~20-fold less active in its ability to induce RNase L cleavage (48). To confirm that the modification of the bromide did not interfere with the binding to the target, we measured the binding affinities of Synucleozid-2.0 (K_d = 66 ± 4 nM), Syn-PA (replacing bromine with propyl amide; K_d = 230 ± 51 nM), Syn-RiboTAC (K_d = 103 ± 10 nM), and Syn-CTRL (K_d = 97 ± 3 nM) for the *SNCA* IRE by microscale thermophoresis (MST). No significant change in K_d was observed for these derivatives of Synucleozid-2.0, and they retained selectivity as no saturable binding was observed for the fully base-paired RNA (*SI Appendix*, Fig. S11).

In the *SNCA*-UTR luciferase reporter assay, both Syn-RiboTAC and Synucleozid-2.0 decreased the luminescence signal dose-dependently to similar extents, with IC_{25}s of 1.2 ± 0.2 μM and 1.6 ± 0.2 μM, respectively (Fig. 4*B* and *SI Appendix*, Fig. S12). Analogous studies using the control luciferase reporter revealed at least 10-fold selectivity toward *SNCA*-IRE (IC_{25}s >10 μM; *SI Appendix*, Fig. S12). While Syn-RiboTAC reduced luciferase activity driven by the *SNCA* IRE by ~40% at the 2 μM dose, Syn-CTRL harboring the less active RNase L regioisomer, only modestly reduced luminescence signal (~10%; Fig. 4*B*), which could be due to its reduced ability to induce RNA cleavage or to inhibiting ribosomal assembly as a binder (same mode of action as Synucleozid-2.0; Fig. 4*B*). Importantly, none of the three compounds inhibited a control luciferase reporter lacking the IRE.

To provide support that inhibition of translation by Syn-RiboTAC was due to RNA cleavage, the abundance of the SNCA *IRE*-luciferase transcript was measured by qRT-PCR. Syn-RiboTAC dose-dependently reduced the transcript's levels by ~50% at 2 μM, while Syn-CTRL had no effect (Fig. 4*C*), confirming that Syn-CTRL inhibits translation through a binding mechanism instead of cleaving the transcript at the 2 μM concentration.

Next, we tested whether Syn-RiboTAC could cleave endogenous *SNCA* mRNA and reduce α-synuclein protein levels in SH-SY5Y cells. Notably, not all *SNCA* transcripts harbor the IRE. Previous RNA-seq studies showed that *SNCA* transcript variants containing the targeted IRE account for ~50% of all detected *SNCA* mRNA species (20). Thus, we expect a maximum reduction of ~50% of total *SNCA* mRNA levels. We designed three sets of primers: one set amplifies the *SNCA* IRE region (measuring all IRE-containing *SNCA* mRNA variants), the second set amplifies a conserved region (measuring total *SNCA* mRNA), and the third set amplifies a region unique to highly expressed non-IRE containing *SNCA* mRNA (measuring the non-IRE containing transcripts). As measured by qRT-PCR, Syn-RiboTAC decreased IRE-containing *SNCA* mRNA levels dose-dependently (48 ± 2% reduction at the maximum concentration of 2 μM; Fig. 4*D*), which corresponds to 29% reduction of total *SNCA* mRNA at the same concentration (Fig. 4*E*). Notably, Syn-RiboTAC showed no effect on non-IRE containing *SNCA* mRNA variants, as they do not have the targeted RNA structure (Fig. 4*E*). A concentration-dependent reduction of α-synuclein protein levels was also observed, down by 63 ± 9% upon treatment with 2 μM of Syn-RiboTAC (Fig. 4*F*), compared to 53 ± 3% by Synucleozid-2.0 at the same concentration (Fig. 2*D* and *E*). Intriguingly, Syn-RiboTAC reduced α-synuclein protein levels to a greater extent than *SNCA* mRNA levels, suggesting that not all transcript variants are translated equally into proteins or that the translating pool of cytoplasmic mRNAs is more selectively degraded with an RNase L RiboTAC (50, 51). It has been shown that a reduction of α-synuclein protein levels by as little as 25% is therapeutically beneficial in a mouse model (52).

Syn-RiboTAC Confers Cytoprotection to SH-SY5Y Cells upon α-Synuclein PFF Challenge. To study the cytoprotective effects of Syn-RiboTAC, we completed the same PFF challenge assay in SH-SY5Y cells that was used for Synucleozid-2.0. As expected from the reduction of α-synuclein protein levels, Syn-RiboTAC protected SH-SY5Y cells dose-dependently from death upon PFF challenge, with 78 ± 16% rescue of cells at the 10 μM dose and an EC_{50} of 2 ± 1 μM (*SI Appendix*, Fig. S13*A*). (Percent rescue was calculated by comparing the number of cells where death was induced by PFFs with and without compound). The cytoprotective effect conferred by Syn-RiboTAC was greater than that of Synucleozid-2.0, which yielded an EC_{50} of 13±4 μM, an ~sixfold difference (*SI Appendix*, Fig. S13*A*). Syn-RiboTAC also had longer-lasting effects than Synucleozid-2.0, as demonstrated by a wash-out experiment, determined from both the PFF challenge assay and the *SNCA*-UTR luciferase reporter assay. In the PFF challenge assay, Syn-RiboTAC demonstrated higher cytoprotective effects than Synucleozid-2.0 at 24 h and 36 h after removal from the cells (*SI Appendix*, Fig. S13*B*). Similarly, in the luciferase reporter assay, Syn-RiboTAC was still active 16 h after its removal from the cells (24 ± 2% inhibition as compared to 34 ± 2% without the wash-out), whereas Synucleozid-2.0 was no longer active (*SI Appendix*, Fig. S13*C*).

Syn-RiboTAC Activity Is RNase L-dependent. To validate mode of action, we knocked down RNase L in SH-SY5Y cells with a pool of siRNAs (*SI Appendix*, Fig. S13*D*), followed by treatment with Syn-RiboTAC. As expected, knocking down RNase L levels ablated the effect of Syn-RiboTAC on *SNCA* mRNA levels, supporting the notion that compound activity is RNase L-dependent (*SI Appendix*, Fig. S13*E*). We also validated that Syn-RiboTAC and Synucleozid-2.0 engage the same binding site in cells by carrying out a competition experiment using a constant concentration of Syn-RiboTAC (2 μM) and varying concentrations of Synucleozid-2.0 (0.1 to 10 μM). A dose-dependent restoration of *SNCA* mRNA levels was observed as a function of Synucleozid-2.0 concentration, suggesting that the two compounds compete for the same A bulge binding pocket of *SNCA* IRE (*SI Appendix*, Fig. S13*F*).

Synucleozid-2.0 and Syn-RiboTAC Are Selective Transcriptome- and Proteome-Wide. Although the *SNCA* IRE A bulge is a rather simple motif, it is not as common as might be expected. Our previous analysis (20) indicates that the *SNCA* IRE A bulge and its closing base pairs are found only five times in the transcriptome, in miR-1207 (Dicer cleavage site), miR-4310 (nonfunctional site), and in three tRNAs, amongst all human RNAs with known structures (n = 7,436 structural elements). To investigate the selectivity of both Syn-RiboTAC and Synucleozid-2.0, we defined all transcripts occupied by the small molecule and then characterized the effect of occupancy transcriptome- and proteome-wide.

To gain initial insight into the selectivity of Syn-RiboTAC at the transcript level, we measured the mRNA levels of other transcripts with IREs in SH-SY5Y cells, including APP, ferritin, and TfR, by qRT-PCR. None of the transcripts was affected by Syn-RiboTAC as they lack the same A bulge as *SNCA* mRNA (Fig. 4*G* and *SI Appendix*, Fig. S5). Similarly, no effect was observed on the protein levels of APP, ferritin, and TfR by Western blot (Fig. 4*H*). These results confirmed that Syn-RiboTAC retained the same specificity for the *SNCA* IRE that Synucleozid-2.0 has.

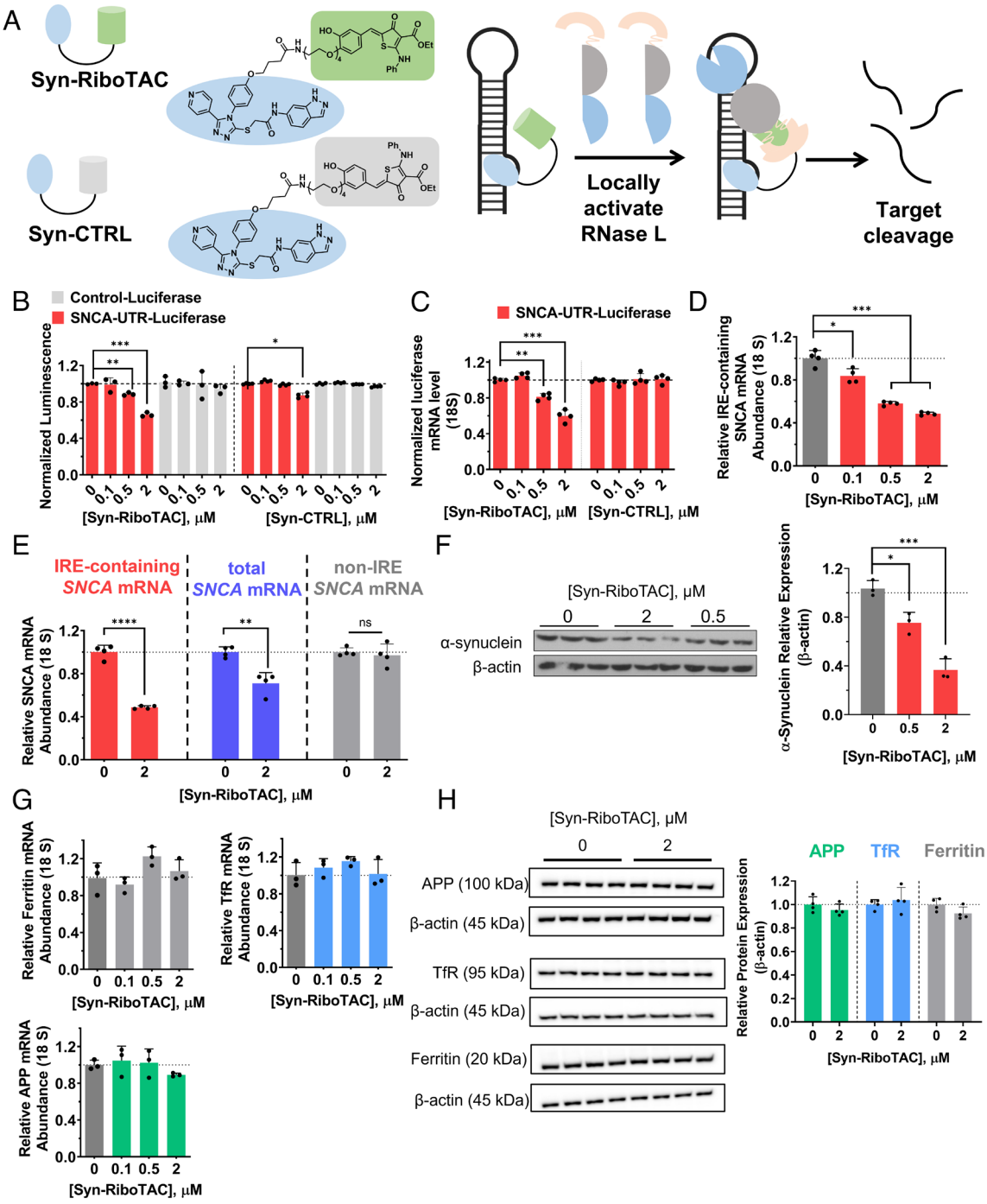

Fig. 4. Syn-RiboTAC selectively degrades *SNCA* mRNA in cells. (*A*) Chemical structures of Syn-RiboTAC, and the control compound, Syn-CTRL, which has a recruiter module that is ~20-fold less active. A schematic of Syn-RiboTAC recruiting RNase L and cleaving *SNCA* mRNA in cells is shown on the right. (*B*) Syn-RiboTAC and Sy-CTRL inhibited SNCA-UTR-Luciferase signal, with no effect on the control luciferase signal that lacks the *SNCA*-UTR sequence (48 h treatment; n = 3 biological replicates for the *SNCA*-UTR Luciferase reporter and n = 4 for the Control Luciferase reporter). (*C*) Syn-RiboTAC decreased luciferase mRNA level for *SNCA*-UTR-Luciferase, while Syn-CTR had no effect on the luciferase mRNA level (48 h treatment; n = 4 biological replicates). (*D*) Syn-RiboTAC cleaved IRE-containing *SNCA* mRNA in SH-SY5Y cells dose-dependently after a 48-h treatment period (n = 4 biological replicates). (*E*) Syn-RiboTAC selectively cleaved IRE-containing *SNCA* mRNA but had no effect on *SNCA* transcript variants lacking the targeted IRE (48 h treatment; n = 4 biological replicates). (*F*) Syn-RiboTAC reduced α-synuclein protein level in SH-SY5Y cells in a dose-dependent manner (48 h treatment; n = 3 biological replicates). (*G*) Syn-RiboTAC had no effect on APP, TfR, or H-Ferritin mRNA levels in SH-SY5Y cells (48 h treatment; n = 3 biological replicates). (*H*) Syn-RiboTAC had no effect on the protein levels of APP, TfR, or H-Ferritin in SH-SY5Y cells (48 h treatment; n = 4 biological replicates). *$P < 0.05$; **$P < 0.01$; ***$P < 0.001$, as determined by two-tailed Student *t* test. Error bars indicate SD.

In unbiased transcriptome-wide studies using RNA-seq, among 30,175 genes detected, Syn-RiboTAC only affected 48 (0.16%) genes (Log_2fold change > 0.58 and $P < 0.05$), with 34 genes down-regulated and 14 genes up-regulated (*SI Appendix*, Fig. S13*G*). Both Syn-RiboTAC and an siRNA targeted to *SNCA* reduced abundance of total *SNCA* transcripts by ~25-30%, although these reductions were not statistically significant by RNA-seq analysis. When measuring the effects on IRE-containing *SNCA* transcripts only, Syn-RiboTAC reduced their abundances by ~50%, consistent with the results measured by qRT-PCR. Notably, *APP*, ferritin, and TfR transcript levels were unaffected in the RNA-seq data (*SI Appendix*, Fig. S13*G*), in accordance with qRT-PCR measurements. There are 690 other

mRNAs that are known to contain IREs in the transcriptome (53). Of these, 447 were detectable in the RNA-seq data, only 19 of which were affected by Syn-RiboTAC treatment (11 down-regulated and eight up-regulated), none of which harbor Syn-RiboTAC/Synucleozid-2.0 binding site in the *SNCA* IRE. Notably, the transcriptome profile of Syn-RiboTAC treatment showed a significant correlation with that of an siRNA targeted to *SNCA* with $R^2 > 0.99$ (*SI Appendix*, Fig. S13 *G–I*). Collectively, these results suggest that Syn-RiboTAC is selective on the transcriptome with limited off-targets.

We also conducted an unbiased proteome-wide analysis. At the proteome level, among 2,813 proteins detected, Synucleozid-2.0 affected 150 (0.53%) proteins, with 55 proteins down-regulated and 95 proteins up-regulated. (α-synuclein was not detected by proteomics due to its low abundance.) Syn-RiboTAC showed similar selectivity, affecting 194 (0.56%) proteins among 3,436 total detected, with 114 proteins down-regulated and 80 up-regulated ($P < 0.05$ with FDR = 1%). Three proteins, *MDH2*, *TCEB2*, and *RBM33*, were up-regulated by both compound treatments. Compared with previous proteomic profiling of Synucleozid 1.0 which affected 8% of global proteins (20), both Synucleozid-2.0 and Syn-RiboTAC showed comparable selectivity with a smaller number of proteins significantly affected (Fig. 5*A*). By comparing RNA-seq and proteomics datasets, a direct correlation between changes in transcript and protein levels can be assessed. Of the 194 proteins that showed changes upon treatment with Syn-RiboTAC, 86 (44%) also showed the corresponding change at the transcript level with modest global correlation (Pearson r = 0.15, $P < 0.05$).

To determine whether the changes observed in the transcriptome and proteome can be traced to direct target engagement, we evaluated the global target engagement of Syn-ChemCLIP followed by transcriptome-wide RNA-seq analysis of all occupied transcripts. These studies revealed that Syn-ChemCLIP enriched (bound) only 107 (0.6%) transcripts (with a minimum enrichment of 1.5-fold and minimum read count of 10) among 18,604 detected in SH-SY5Y cells (*SI Appendix*, Fig. S13*J*). Among these 107 enriched transcripts, only two (*SNCA* and *TAGLN*) are known to contain IREs. Syn-RiboTAC showed no effect on *TAGLN* mRNA levels (*SI Appendix*, Fig. S13*K*), and neither Synucleozid-2.0 nor Syn-RiboTAC affected *TAGLN* protein abundance (Fig. 5 *B* and *C*).

Comparing transcriptome-wide Chem-CLIP studies with RNA-seq data of Syn-RiboTAC revealed that none of the 11 transcripts containing IREs that were reduced by Syn-RiboTAC [validated by qRT-PCR measurements (*SI Appendix*, Fig. S14)] were bound by Syn-ChemCLIP. Of the 107 bound transcripts, 38 were detected in the RNA-seq analysis of Syn-RiboTAC; the levels of only four (including *SNCA*) were reduced (cleaved) by Syn-RiboTAC treatment (*SI Appendix*, Fig. S13*K*). Of the three other transcripts, one (*NEAT1)* is a long noncoding (lnc) RNA while the other two (*HHIPL1* and *MYO15B*) were not detectable in the proteomics data, whether vehicle- or RiboTAC-treated. By Western blotting, the levels of *HHIPLI* and *MYO15B* were only modestly reduced (~20%; *SI Appendix*, Fig. S15).

Of the remaining 34 transcripts bound by the small molecule and detectable in the RNA-seq data where their levels were generally unaffected (*BLVRB* was reduced by a statistically nonsignificant ~20%; *SI Appendix*, Fig. S13*K*), the proteins encoded by seven of them were detectable by global proteomics. Expression levels of these proteins were not significantly altered by Synucleozid-2.0 (Fig. 5*B*) or Syn-RiboTAC treatment (Fig. 5*C*), and this finding was verified by Western blotting (*SI Appendix*, Fig. S16). No correlation ($P > 0.1$ with Pearson correlation test) was observed between enrichment by Syn-ChemCLIP and the change in protein abundance upon treatment with either Synucleozid-2.0 or Syn-RiboTAC, confirming that not all target engagements elicited a downstream effect.

Synucleozid-2.0 and Syn-RiboTAC Reduce α-Synuclein Protein Levels in Dopaminergic Neurons. We next tested Synucleozid-2.0 and Syn-RiboTAC in human dopaminergic neurons as their degeneration is a key hallmark of PD (54). Dopaminergic neurons were differentiated from induced pluripotent stem cells (iPSCs) obtained from either a PD patient with *SNCA* triplication or a healthy individual. At 2 μM, both compounds decreased α-synuclein protein levels by ~50%, lowering the elevated levels of α-synuclein in patient-derived neurons to a level similar to that observed in healthy, untreated neurons (Fig. 5*D*). Notably, Synucleozid-2.0 had no effect on the *SNCA* mRNA levels while Syn-RiboTAC decreased transcript levels by ~50%, consistent with their respective mechanisms of action (Fig. 5*E*).

Total RNA-seq to evaluate the global effects of Syn-RiboTAC in PD patient–derived dopaminergic neurons revealed only one gene besides *SNCA*, hexokinase 2 (*HK2*), which does not harbor an IRE, was decreased significantly by Syn-RiboTAC treatment (*SI Appendix*, Fig. S13*L*). Interestingly, *HK2* is known to promote apoptosis of dopaminergic neurons in PD (55) and, thus its decrease could alleviate neuronal degeneration in PD. Among 976 genes that were significantly up-regulated in PD patient–derived neurons as compared to those derived from a healthy donor (Log2FoldChange > 1 and $P < 0.05$), 488 (50%) were improved by treatment with Syn-RiboTAC (Log_2FoldChange > 1 and $P < 0.05$); the abundance of 28 genes was reduced by >50%. Similarly, among 461 genes significantly down-regulated in PD patient-derived neurons (Log_2FoldChange > 1 and $P < 0.05$), 223 (48%) improved by treatment with Syn-RiboTAC (Log_2FoldChange > 1 and $P < 0.05$; Fig. 5*F*) with 31 genes increased by >50%. Overall, Syn-RiboTAC rescued expression of about half of the genes dysregulated in PD patient–derived dopaminergic neurons.

Since α-synuclein protein levels were not detected by proteomics in SHSY-5Y cells, we also performed a global proteomics study in iPSCs derived from a PD patient and from a healthy donor (*SI Appendix*, Fig. S17*A*). Comparing the proteomic profiles of iPSC from the healthy donor and from the PD patient revealed that amongst 6,903 proteins detected, the abundance of 53 proteins (0.8%) were up-regulated and 111 proteins were down-regulated (1.6%) ($P < 0.05$ with FRD = 1%). As expected, α-synuclein protein levels were ~threefold higher in patient-derived iPSCs than those from a healthy donor, in agreement with measurements by ELISA (Fig. 5*D*). Notably, α-synuclein protein levels were reduced by twofold upon Syn-RiboTAC treatment, as quantified by global proteomics. Supporting the selectivity of Syn-RiboTAC (2 μM, 48 h), only 152 (2.2%) proteins were affected overall, with the abundance of 86 increased and 66 reduced (*SI Appendix*, Fig. S17*B*), similar to global proteomics studies completed in SHSY-5Y cells (Fig. 5*A*). Importantly, these changes in protein abundance reflect an overall improvement of the proteomic profile of patient-derived iPSCs. That is, of the 53 proteins with increased abundance in patient-derived iPSCs, 51 were reduced (~96%), 24 of which were reduced by >50%. Similarly, amongst the 111 down-regulated proteins, 102 were increased upon Syn-RiboTAC treatment (~92%), 58 of which were increased by >50%.

In transcriptome-wide studies, Syn-RiboTAC reduced the aberrant upregulation of 28 genes by >50%. Of these one, *COLEC11*, was also detected by global proteomics, showing a ~25% reduction in protein levels. A previous study has shown *COLEC11* is a causal gene for PD (56). The RiboTAC also boosted the levels of 31 genes

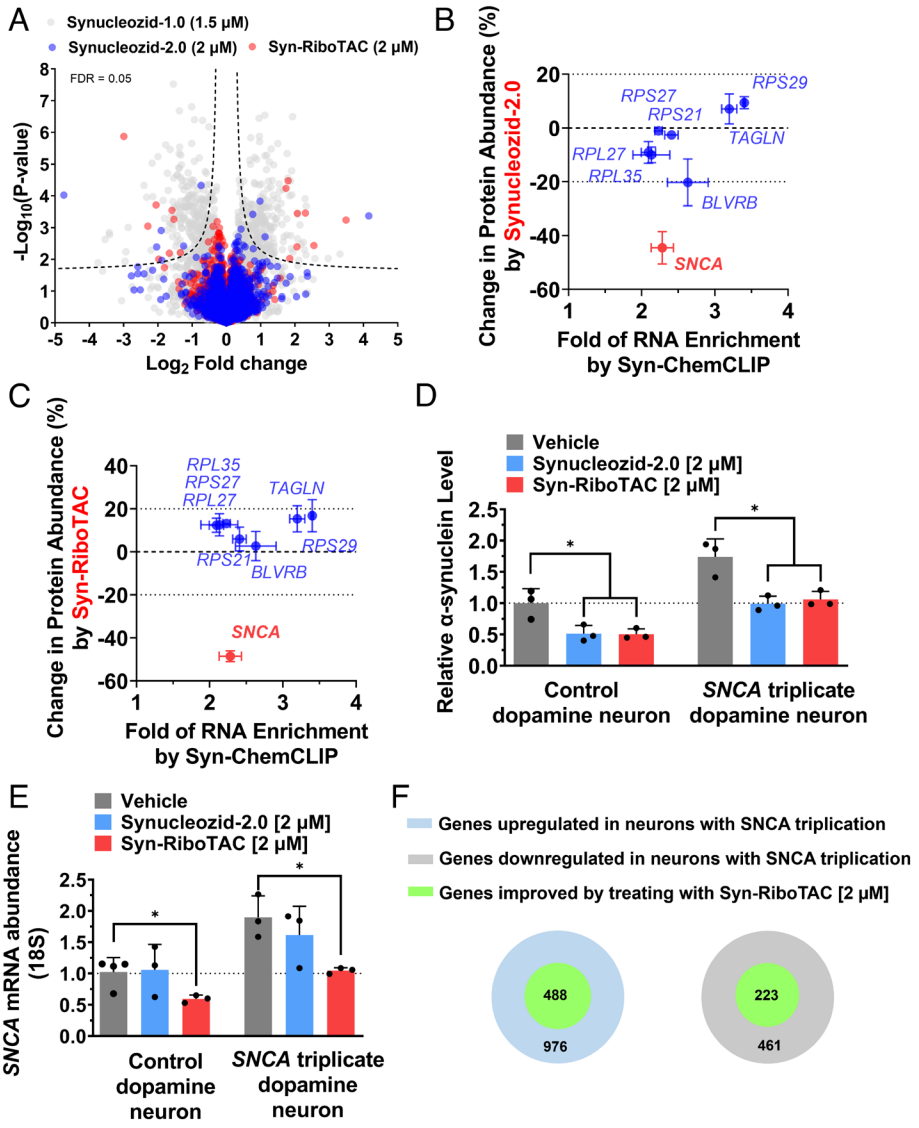

Fig. 5. Synucleozid-2.0 and Syn-RiboTAC are selective on the proteome and reduce α-synuclein protein abundance in PD patient-derived dopaminergic neurons. (*A*) Global proteomics for SH-SY5Y cells treated with Synucleozid-1.0 (1.5 μM), Synucleozid-2.0 (2 μM), and Syn-RIBOTAC (2 μM) for 48 h (n = 3 biological replicates). Dotted lines indicate a false discovery rate (FDR) of 1%. Among 2,813 proteins detected, Synucleozid-2.0 affected 150 (0.53%) proteins, with 55 proteins down-regulated and 95 proteins up-regulated. Syn-RiboTAC showed similar selectivity by affecting 194 (0.56%) proteins among 3,436 total detected, with 114 proteins down-regulated and 80 up-regulated. (*B*) Protein expression levels detectable by proteomics (shown on *Y* axis) of seven genes enriched by Syn-ChemCLIP after a 16-h treatment period (shown on *X* axis) were not affected by Synucleozid-2.0 (2 μM) treatment (n = 3 biological replicates). (*C*) Protein expression levels detectable by proteomics of seven genes enriched by Syn-ChemCLIP are not affected by Syn-RiboTAC (2 μM) treatment (n = 3 biological replicates). (*D*) Synucleozid-2.0 and Syn-RiboTAC decreased α-synuclein protein levels in human iPSC-derived dopaminergic neurons as determined by ELISA (48 h treatment; n = 3 biological replicates). (*E*) Syn-RiboTAC decreased *SNCA* mRNA levels while Synucleozid-2.0 had no effect in iPSC-derived dopaminergic neurons (48 h treatment; n = 3 biological replicates except for vehicle-treated control dopaminergic neurons where n = 4 biological replicates). (*F*) Syn-RiboTAC normalized expression level of about half of the genes in dopaminergic neurons differentiated from PD patient–derived iPSC cells by converging them toward the levels observed in neurons from a control individual after a 48-h treatment period (n = 3 biological replicates). $*P < 0.05$; $**P < 0.01$; $***P < 0.001$, as determined by two-tailed Student *t* test. Error bars indicate SD.

that were aberrantly down-regulated in PD patient-derived iPSCs. None was detected by global proteomics due to their low protein abundances; four were noncoding genes that are not translated.

Conclusions and Implications

We have presented an integrated approach to define drug-like chemical matter that affects RNA by simple binding and by targeted degradation, as applied to targeting the *SNCA* mRNA. Importantly, small-molecule binding selectively inhibits translation of the mRNA, reducing levels of α-synuclein protein, a difficult-to-target IDP. Both antibodies (57) and ASOs (52) have been employed, the former to target extracellular α-synuclein, for therapeutic intervention of PD. One advantage of the small molecule approach presented herein is the potential for oral bioavailability and to target intracellular α-synuclein in both central and peripheral systems. Much work remains to test this hypothesis, however.

To meet many unmet medical needs, expanding druggability and developing the tools to do so will be required. We showed that an undruggable protein can be modulated by targeting its encoding mRNA and developed a streamlined workflow to define and study these compounds. This approach could be broadly applicable and includes targeting structural elements throughout an mRNA. The demonstration that targeting RNA structural elements near a start codon is effective to modulate biology suggests that such elements may be important general targetable sites.

Nature has evolved processes that allow small molecules to control the structural switching of bacterial RNAs to regulate production of metabolites, and these riboswitches are the targets of antibacterials (58, 59). This study gives credence to the assertion that small molecules can target human RNA structural elements and impart riboswitch-like control to translation by using exogenously delivered small molecules (60, 61). In addition, as the defined mode of action of Synucleozid-2.0 is to pause ribosome assembly, the small molecule is a useful chemical tool to better study this process. Further, we demonstrated that one way to enhance the bioactivity while retaining the selectivity of small molecules targeting RNA is to convert simple RNA binders to RiboTAC degraders. Importantly, RiboTACs do not require binding to functional sites to elicit activity as is the case for small molecules with binding mechanisms of action; rather, they can bind biologically inert sites and induce their degradation by endogenous nucleases. The most common way to elicit functional effects to eliminate disease-causing RNAs is by using oligonucleotide modalities, many of which have achieved FDA-approval. However, these large molecular weight compounds can have limited tissue distribution, are injected medicines, and have poor brain penetrance. The approach herein for targeted RNA degradation using heterobifunctional molecules

could be further advanced to provide molecules with broader tissue distribution that could also be developed into orally bioactive medicines. Although much work remains in this area, these studies could lay a foundation to achieve these goals.

Materials and Methods

Characterization of in vitro binding and target engagement were completed by a 2-AP fluorescence-based assay, microscale thermophoresis, thermal melting analysis, Chem-CLIP, Chem-CLIP-Map-Seq, and ASO-Bind-Map. Cellular activity, selectivity, and target engagement were assessed using luciferase reporters, Western blotting of endogenous a-synuclein, qRT-PCR, cytoprotection against PFFs, cellular viability, Chem-CLIP, ASO-Bind-Map, and global transcriptome-wide and proteome-wide analysis. Complete methods can be found at *SI Appendix*.

Quantification and Statistical Analysis. All data are reported as means with error bars representing SD, unless noted otherwise. Statistical tests and number of replicates (*n*) are noted in each figure legend. Data were plotted using GraphPad Prism 7 software, which was also used to calculate statistical significance.

Data, Materials, and Software Availability. All data including global proteomics and RNA-seq studies are available on Mendeley Data (DOI: 10.17632/pmtjyvmvn8.1) (62). No unique codes or software were used in this study. Detailed methods for all experiments in this manuscript can be found in *SI Appendix*.

ACKNOWLEDGMENTS. This work was funded by the NIH (R21/R33NS096032 to M.M.M. and M.D.D.; R01GM097455, DP1NS096898, and R35NS116846 to M.D.D.). We also thank the Nelson Family Fund and Ed and Jane Greenberg. M.M.M. is the William Dow Lovett Professor of Neurology and is supported by the Michael J. Fox Foundation for Parkinson's Research, American Parkinson Disease Association, and NIH Grants R01NS101134, RF1NS130702, UG3/UH3NS116921, R21NS123770 and R21AG075656. We thank Dr. Yoshihiro Akahori for aiding in the synthesis of small molecules used in this study.

Author affiliations: [a]Department of Chemistry, The Scripps Research Institute, Jupiter, FL 33458; [b]Department of Chemistry, The Herbert Wertheim UF Scripps Institute for Biomedical Innovation & Technology, Jupiter, FL 33458; [c]Rutgers Robert Wood Johnson Medical School Institute for Neurological Therapeutics, Piscataway, NJ 08854; and [d]Department of Neurology, Rutgers Robert Wood Johnson Medical School, Piscataway, NJ 08854

1. M. Clamp *et al.*, Distinguishing protein-coding and noncoding genes in the human genome. *Proc. Natl. Acad. Sci. U.S.A.* **104**, 19428–19433 (2007), 10.1073/pnas.0709013104.
2. A. L. Hopkins, C. R. Groom, The druggable genome. *Nat. Rev. Drug Discov.* **1**, 727–730 (2002), 10.1038/nrd892.
3. G. M. Burslem, C. M. Crews, Proteolysis-targeting chimeras as therapeutics and tools for biological discovery. *Cell* **181**, 102–114 (2020), 10.1016/j.cell.2019.11.031.
4. A. C. Lai, C. M. Crews, Induced protein degradation: An emerging drug discovery paradigm. *Nat. Rev. Drug Discov.* **16**, 101–114 (2017), 10.1038/nrd.2016.211.
5. K. M. Sakamoto *et al.*, Protacs: Chimeric molecules that target proteins to the Skp1-Cullin-F box complex for ubiquitination and degradation. *Proc. Natl. Acad. Sci. U.S.A.* **98**, 8554–8559 (2001), 10.1073/pnas.141230798.
6. K. M. Sakamoto *et al.*, Development of Protacs to target cancer-promoting proteins for ubiquitination and degradation. *Mol. Cell Proteomics* **2**, 1350–1358 (2003), 10.1074/mcp.T300009-MCP200.
7. M. Kostic, L. H. Jones, Criticalassessment of targeted protein degradation as a research tool and pharmacological modality. *Trends Pharmacol. Sci.* **41**, 305–317 (2020), 10.1016/j.tips.2020.02.006.
8. J. M. Ostrem, K. M. Shokat, Direct small-molecule inhibitors of KRAS: From structural insights to mechanism-based design. *Nat. Rev. Drug Discov.* **15**, 771–785 (2016), 10.1038/nrd.2016.139.
9. J. Rudolph, D. Stokoe, Selective inhibition of mutant Ras protein through covalent binding. *Angew. Chem. Int. Ed. Engl.* **53**, 3777–3779 (2014), 10.1002/anie.201400233.
10. S. Kamerkar *et al.*, Exosomes facilitate therapeutic targeting of oncogenic KRAS in pancreatic cancer. *Nature* **546**, 498–503 (2017), 10.1038/nature22341.
11. B. A. Lanman *et al.*, Discovery of a covalent inhibitor of KRAS(G12C) (AMG 510) for the treatment of solid tumors. *J. Med. Chem.* **63**, 52–65 (2020), 10.1021/acs.jmedchem.9b01180.
12. J. L. Counihan, B. Ford, D. K. Nomura, Mapping proteome-wide interactions of reactive chemicals using chemoproteomic platforms. *Curr. Opin. Chem. Biol.* **30**, 68–76 (2016), 10.1016/j.cbpa.2015.11.007.
13. S. L. Schreiber *et al.*, Advancing biological understanding and therapeutics discovery with small-molecule probes. *Cell* **161**, 1252–1265 (2015), 10.1016/j.cell.2015.05.023.
14. V. M. Lee, J. Q. Trojanowski, Mechanisms of Parkinson's disease linked to pathological alpha-synuclein: New targets for drug discovery. *Neuron* **52**, 33–38 (2006), 10.1016/j.neuron.2006.09.026.
15. K. C. Luk *et al.*, Pathological alpha-synuclein transmission initiates Parkinson-like neurodegeneration in nontransgenic mice. *Science* **338**, 949–953 (2012), 10.1126/science.1227157.
16. A. B. Singleton *et al.*, alpha-Synuclein locus triplication causes Parkinson's disease. *Science* **302**, 841 (2003), 10.1126/science.1090278.
17. D. M. Maraganore, Rationale for therapeutic silencing of alpha-synuclein in Parkinson's disease. *J Mov. Disord.* **4**, 1–7 (2011).
18. C. A. Ross, M. A. Poirier, Protein aggregation and neurodegenerative disease. *Nat. Med.* **10**, S10–S17 (2004), 10.1038/nm1066.
19. M. R. Naylor, A. T. Bockus, M. J. Blanco, R. S. Lokey, Cyclic peptide natural products chart the frontier of oral bioavailability in the pursuit of undruggable targets. *Curr. Opin. Chem. Biol.* **38**, 141–147 (2017), 10.1016/j.cbpa.2017.04.012.
20. P. Zhang *et al.*, Translation of the intrinsically disordered protein alpha-synuclein is inhibited by a small molecule targeting its structured mRNA. *Proc. Natl. Acad. Sci. U.S.A.* **117**, 1457–1467 (2020), 10.1073/pnas.1905057117.
21. J. L. Childs-Disney *et al.*, Targeting RNA structures with small molecules. *Nat. Rev. Drug Discov.* **21**, 736–762 (2022), 10.1038/s41573-022-00521-4.
22. Y. Tong *et al.*, Transcriptome-wide mapping of small-molecule RNA-bindingsites in cells informs an isoform-specific degrader of QSOX1 mRNA. *J. Am. Chem. Soc.* **144**, 11620–11625 (2022), 10.1021/jacs.2c01929.
23. A. L. Friedlich, R. E. Tanzi, J. T. Rogers, The 5′-untranslated region of Parkinson's disease alpha-synuclein messengerRNA contains a predicted iron responsive element. *Mol. Psychiatry* **12**, 222–223 (2007), 10.1038/sj.mp.4001937.
24. Z. D. Zhou, E. K. Tan, Iron regulatory protein (IRP)-iron responsive element (IRE) signaling pathway in human neurodegenerative diseases. *Mol. Neurodegener.* **12**, 75 (2017), 10.1186/s13024-017-0218-4.
25. T. T. Wager, X. Hou, P. R. Verhoest, A. Villalobos, Moving beyond rules: The development of a central nervous system multiparameter optimization (CNS MPO) approach to enable alignment of druglike properties. *ACS Chem. Neurosci.* **1**, 435–449 (2010), 10.1021/cn100008c.
26. M. D. Disney *et al.*, Inforna 2.0: A Platform for the sequence-based design of small molecules targeting structured RNAs. *ACS Chem. Biol.* **11**, 1720–1728 (2016), 10.1021/acschembio.6b00001.
27. S. P. Velagapudi *et al.*, Approved anti-cancer drugs target oncogenic non-coding RNAs. *Cell Chem. Biol.* **25**, 1086–1094.e1087 (2018), 10.1016/j.chembiol.2018.05.015.
28. H. S. Haniff, A. Graves, M. D. Disney, Selective small molecule recognition of RNA base pairs. *ACS Combi. Sci.* **20**, 482–491 (2018), 10.1021/acscombsci.8b00049.
29. S. P. Velagapudi, S. M. Gallo, M. D. Disney, Sequence-based design of bioactive small molecules that target precursor microRNAs. *Nat. Chem. Biol.* **10**, 291–297 (2014), 10.1038/nchembio.1452.
30. S. P. Velagapudi *et al.*, Design of a small molecule against an oncogenic noncoding RNA. *Proc. Natl. Acad. Sci. U.S.A.* **113**, 5898–5903 (2016), 10.1073/pnas.1523975113.
31. M. G. Costales *et al.*, Small molecule inhibition of microRNA-210 reprograms an oncogenic hypoxic circuit. *J. Am. Chem. Soc.* **139**, 3446–3455 (2017), 10.1021/jacs.6b11273.
32. M. G. Costales *et al.*, A designed small molecule inhibitor of a non-coding RNA sensitizes HER2 negative cancers to Herceptin. *J. Am. Chem. Soc.* **141**, 2960–2974 (2019), 10.1021/jacs.8b10558.
33. H. Xicoy, B. Wieringa, G. J. Martens, The SH-SY5Y cell line in Parkinson's disease research: A systematic review. *Mol. Neurodegener.* **12**, 10 (2017), 10.1186/s13024-017-0149-0.
34. R. S. Eisenstein, Iron regulatory proteins and the molecular control of mammalian iron metabolism. *Annu. Rev. Nutr.* **20**, 627–662 (2000), 10.1146/annurev.nutr.20.1.627.
35. L. A. Volpicelli-Daley *et al.*, Exogenous alpha-synuclein fibrils induce Lewy body pathology leading to synaptic dysfunction and neuron death. *Neuron* **72**, 57–71 (2011), 10.1016/j.neuron.2011.08.033.
36. H. H. Cho *et al.*, Selective translational control of the Alzheimer amyloid precursor protein transcript by iron regulatory protein-1. *J. Biol. Chem.* **285**, 31217–31232 (2010), 10.1074/jbc.M110.149161.
37. D. N. Rupani, G. J. Connell, Transferrin receptor mRNA interactions contributing to iron homeostasis. *Rna* **22**, 1271–1282 (2016), 10.1261/rna.056184.116.
38. J. M. Jean, K. B. Hall, 2-Aminopurine fluorescence quenching and lifetimes: Role of base stacking. *Proc. Natl. Acad. Sci. U.S.A.* **98**, 37–41 (2001), 10.1073/pnas.98.1.37.
39. M. Kaul, C. M. Barbieri, D. S. Pilch, Fluorescence-based approach for detecting and characterizing antibiotic-induced conformational changes in ribosomal RNA: Comparing aminoglycoside binding to prokaryotic and eukaryotic ribosomal RNA sequences. *J. Am. Chem. Soc.* **126**, 3447–3453 (2004), 10.1021/ja030568i.
40. S. Shandrick *et al.*, Monitoring molecular recognition of the ribosomal decoding site. *Angew. Chem. Int. Ed. Engl.* **43**, 3177–3182 (2004), 10.1002/anie.200454217.
41. P. P. Zarrinkar, J. R. Williamson, Kinetic intermediates in RNA folding. *Science* **265**, 918–924 (1994), 10.1126/science.8052848.
42. S. P. Velagapudi, Y. Li, M. D. Disney, A cross-linking approach to map small molecule–RNA binding sites in cells. *Bioorg. Med. Chem. Lett.* **29**, 1532–1536 (2019), 10.1016/j.bmcl.2019.04.001.
43. G. M. Brittenham *et al.*, Efficacy of deferoxamine in preventing complications of iron overload in patients with thalassemia major. *N. Engl. J. Med.* **331**, 567–573 (1994), 10.1056/NEJM199409013310902.
44. B. Guo, J. D. Phillips, Y. Yu, E. A. Leibold, Iron regulates the intracellular degradation of iron regulatory protein 2 by the proteasome. *J. Biol. Chem.* **270**, 21645–21651 (1995), 10.1074/jbc.270.37.21645.
45. H. Chasse, S. Boulben, V. Costache, P. Cormier, J. Morales, Analysis of translation using polysome profiling. *Nucleic Acids Res.* **45**, e15 (2017), 10.1093/nar/gkw907.
46. C. Pena, E. Hurt, V. G. Panse, Eukaryotic ribosome assembly, transport and quality control. *Nat. Struct. Mol. Biol.* **24**, 689–699 (2017), 10.1038/nsmb.3454.
47. T. T. Wager, X. Hou, P. R. Verhoest, A. Villalobos, Central nervous system multiparameter optimization desirability: Application in drug discovery. *ACS Chem. Neurosci.* **7**, 767–775 (2016), 10.1021/acschemneuro.6b00029.
48. M. G. Costales *et al.*, Small-molecule targeted recruitment of a nuclease to cleave an oncogenic RNA in a mouse model of metastatic cancer. *Proc. Natl. Acad. Sci. U.S.A.* **117**, 2406–2411 (2020), 10.1073/pnas.1914286117.

49. P. Zhang *et al.*, Reprogramming of protein-targeted small-molecule medicines to RNA by ribonuclease recruitment. *J. Am. Chem. Soc.* **143**, 13044–13055 (2021), 10.1021/jacs.1c02248.
50. Y. Liu, A. Beyer, R. Aebersold, On the dependency of cellular protein levels on mRNA abundance. *Cell* **165**, 535–550 (2016), 10.1016/j.cell.2016.03.014.
51. B. Schwanhausser *et al.*, Global quantification of mammalian gene expression control. *Nature* **473**, 337–342 (2011), 10.1038/nature10098.
52. D. Alarcon-Aris *et al.*, Anti-alpha-synuclein ASO delivered to monoamine neurons prevents alpha-synuclein accumulation in a Parkinson's disease-like mouse model and in monkeys. *EBioMedicine* **59**, 102944 (2020), 10.1016/j.ebiom.2020.102944.
53. S. D. Baird, M. Turcotte, R. G. Korneluk, M. Holcik, Searching for IRES. *RNA* **12**, 1755–1785 (2006), 10.1261/rna.157806.
54. M. Naoi, W. Maruyama, Cell death of dopamine neurons in aging and Parkinson's disease. *Mech. Ageing. Dev.* **111**, 175–188 (1999), 10.1016/s0047-6374(99)00064-0.
55. J. Li *et al.*, Upregulated hexokinase 2 expression induces the apoptosis of dopaminergic neurons by promoting lactate production in Parkinson's disease. *Neurobiol. Dis.* **163**, 105605 (2022), 10.1016/j.nbd.2021.105605.
56. S. Kaiser *et al.*, A proteogenomic view of Parkinson's disease causality and heterogeneity. *NPJ Parkinsons Dis.* **9**, 24 (2023), 10.1038/s41531-023-00461-9.
57. A. Weihofen *et al.*, Development of an aggregate-selective, human-derived alpha-synuclein antibody BIIB054 that ameliorates disease phenotypes in Parkinson's disease models. *Neurobiol. Dis.* **124**, 276–288 (2019), 10.1016/j.nbd.2018.10.016.
58. J. A. Howe *et al.*, Selective small-molecule inhibition of an RNA structural element. *Nature* **526**, 672–677 (2015), 10.1038/nature15542.
59. A. Serganov, A. Polonskaia, A. T. Phan, R. R. Breaker, D. J. Patel, Structural basis for gene regulation by a thiamine pyrophosphate-sensing riboswitch. *Nature* **441**, 1167–1171 (2006), 10.1038/nature04740.
60. C. A. O'Leary *et al.*, RNA structural analysis of the MYC mRNA reveals conserved motifs that affect gene expression. *PLoS One* **14**, e0213758 (2019), 10.1371/journal.pone.0213758.
61. J. L. Chen *et al.*, The RNA encoding the microtubule-associated protein tau has extensive structure that affects its biology. *PLoS One* **14**, e0219210 (2019), 10.1371/journal.pone.0219210.
62. Y. Tong, P. Zhang, J. Liu, M. M. Mouradian, M. Disney, Small molecule targeting α-synuclein mRNA. Mendeley Data. https://data.mendeley.com/datasets/pmtjyvmvn8/1. Deposited 10 May 2023.